

Semantic-aware Occlusion Filtering Neural Radiance Fields in the Wild

Jaewon Lee¹ Injae Kim¹ Hwan Heo¹ Hyunwoo J. Kim^{1*}

¹Korea University

{2j1eju, dna9041, gjghks950, hyunwoojkim}@korea.ac.kr

Abstract

We present a learning framework for reconstructing neural scene representations from a small number of unconstrained tourist photos. Since each image contains transient occluders, decomposing the static and transient components is necessary to construct radiance fields with such in-the-wild photographs where existing methods require a lot of training data. We introduce SF-NeRF, aiming to disentangle those two components with only a few images given, which exploits semantic information without any supervision. The proposed method contains an occlusion filtering module that predicts the transient color and its opacity for each pixel, which enables the NeRF model to solely learn the static scene representation. This filtering module learns the transient phenomena guided by pixel-wise semantic features obtained by a trainable image encoder that can be trained across multiple scenes to learn the prior of transient objects. Furthermore, we present two techniques to prevent ambiguous decomposition and noisy results of the filtering module. We demonstrate that our method outperforms state-of-the-art novel view synthesis methods on Phototourism dataset in a few-shot setting.

1. Introduction

In recent years, synthesizing novel views from 2D images has received increasing attention due to the rapid development of neural rendering techniques. Particularly, neural radiance fields (NeRF) [1] has shown remarkable performance on novel view synthesis by implicitly encoding volumetric density and color of a 3D scene through a multi-layer perceptron (MLP). With the success of NeRF, several subsequent works have been proposed to extend the neural field to speed up training and rendering [2–7], handle dynamic scenes [8–16], learn scene representation with few images [17–27] and so on. However, most of these approaches have been demonstrated in controlled settings, where the radiance of the scene across all images does not

change and every content in the scene is static. In the case of real-world images (e.g., internet photographs of cultural landmarks), they don't follow this assumption: the illumination varies depending on the time and weather the photo was taken, and moving objects such as clouds, people or cars could appear.

A number of studies have conducted to handle the photometric variation and transient objects. Previous works have mainly addressed the inconsistent appearance by using an appearance embedding for each image and optimizing them [28–30]. As for the transient phenomena which we will focus on, NeRF-W [28] and HA-NeRF [31] utilize an additional transient module that separates transient components from the scene. On the other hand, Block-NeRF [29] and Mega-NeRF [30] use segmentation models to mask out objects of classes that are generally considered as movable objects. However, the former requires a large number of images since the model has to get rid of the occluders as well as to learn the complicated geometry and appearance of the scene, and the latter is restricted to predefined classes, which could miss exceptional objects such as shadows.

To address these limitations, we propose a novel framework named SF-NeRF, which utilizes two additional modules: an image encoder that learns the prior of transient occluders and an occlusion filtering module called FilterNet. FilterNet decomposes static and transient phenomena by predicting the transient components: color and opacity for each image, conditioned on the image feature given by the encoder. In contrast to the previous methods above, our method is not constrained to predefined classes and can learn features that can be generally used to disentangle transient objects from the scene, which enables few-shot learning. Moreover, we apply a reparameterization technique to the transient opacity by modeling it as a Binary Concrete random variable to separate transient objects from the scene completely. We also add a regularization term to impose smoothness constrain on the transient opacity.

We evaluate our method on Phototourism dataset [32], which includes internet photos taken at cultural landmarks, under the few-shot setting, training with 30 images for each landmark. Our experiments demonstrate that SF-NeRF can

*corresponding author.

learn the prior of transient occluders and thus decompose the scene with only a few training images.

In summary, our contributions can be summarized as follows:

- We propose a novel framework (SF-NeRF) that learns to decompose static and transient components of the scene by exploiting semantic features of the images in an unsupervised manner.
- We introduce a reparameterization technique within FilterNet during training to avoid ambiguous decomposition of the scene.
- We introduce a regularization term to ensure the smoothness of transient opacity field.
- The proposed method outperforms state-of-the-art novel view synthesis methods on Phototourism dataset under the few-shot setting.

2. Related Works

2.1. Neural Rendering

In recent years, neural scene representations have been extensively studied to achieve novel view synthesis and 3D reconstruction tasks [1, 33–40]. In particular, neural radiance fields (NeRF) [1] represents a 3D scene by combining differentiable volume rendering with MLPs and achieves photorealistic novel view synthesis. After the great success of the NeRF, several subsequent works have attempted to improve its performance on view synthesis [3, 41, 42] or extend it to solve other neural rendering tasks such as generative tasks [43–47], fast rendering [2, 4–7, 48], few-shot view synthesis [17, 18, 20–23, 25, 27, 49], pose estimation [50–53], dynamic view synthesis [8–16], relighting [54–57] and so on. Martin-Brualla *et al.* [28] and Chen *et al.* [31] aim to solve view synthesis with internet photo collections which contain transient occluding subjects and variable illumination. Our work focus on training with these photos in a few-shot setting.

2.2. 3D scene decomposition

Research towards scene decomposition has been conducted for various purposes. A number of studies separate foreground and background NeRF models in order to handle unbounded scenes for outdoor environments [30, 58, 59]. In the case of dynamic scenes, several works decompose static NeRF model for the background and dynamic NeRF for the foreground, which includes objects that move within the scene [12–14, 60, 61]. Some studies aim to decompose scenes consisting of multiple objects [29, 30, 59, 62–68] and further manipulate those objects separately [62–65] with the help of external knowledge such as segmentation features [63] or masks [29, 30, 59, 62, 64, 65].

Reconstructing 3D scenes from photo collections taken in real-world environments such as the Phototourism dataset [32] is challenging since the scene is occluded by various objects in most images. Therefore, disentangling the transient elements from the static scene is essential. NeRF-W [28] address this by adding a “transient” head to the NeRF model that emits its own color and density conditioned on image-wise embeddings. Instead of reconstructing transient objects by using a 3D transient field, HA-NeRF [31] replace it with an image-dependent 2D visibility map which masks out the transient part of the image. However, NeRF-W [28] and HA-NeRF [31] cannot decompose static and transient components when a small number of training images are given. We aim to focus on disentangling transient components from the scene with few images.

3. Methods

We propose a novel learning framework, named as “Semantic-aware Occlusion Filtering Neural Radiance Fields (SF-NeRF)”, to learn NeRF representations from only a few in-the-wild photographs. In order to decompose static and transient components consistently, we introduce a new occlusion handling module called FilterNet, which predicts the transient components with the help of semantic information of the images extracted by an unsupervised pre-trained encoder in Sec. 3.2. We then use one reparameterization trick to avoid ambiguous decomposition in Sec. 3.3. During training, we employ a prior to prevent FilterNet’s noisy results in Sec. 3.4. Our overall pipeline is illustrated in Figure 1.

3.1. Preliminary

Before introducing SF-NeRF, we first briefly review NeRF and its relevant methods we use for reconstructing static scene. We adopt a conditional NeRF structure of which the emitted radiance is conditioned on an image-wise latent embedding. Moreover, we use Integrated Positional Encoding (IPE) that featurizes a region of space instead of a single point, enabling a single MLP to learn multiscale scene representation.

Neural Radiance Fields (NeRF). NeRF [1] represents a scene with a continuous volumetric radiance field F_θ by using a multi-layer perceptron (MLP). Given a 3D position $\mathbf{x} = (x, y, z) \in \mathbb{R}^3$ and a viewing direction $\mathbf{d} \in \mathbb{S}^2$, the NeRF network F_θ returns a volume density σ and an emitted color $\mathbf{c} = (r, g, b)$.

$$\begin{aligned} [\sigma, \mathbf{z}] &= \text{MLP}_{\theta_1}(\gamma_{\mathbf{x}}(\mathbf{x})), \\ \mathbf{c} &= \text{MLP}_{\theta_2}(\gamma_{\mathbf{d}}(\mathbf{d}), \mathbf{z}), \end{aligned} \quad (1)$$

where $\theta = [\theta_1, \theta_2]$ are trainable parameters of MLPs, $\gamma_{\mathbf{x}}(\cdot)$ and $\gamma_{\mathbf{d}}(\cdot)$ are the pre-defined encoding functions [1] for spa-

tial position and viewing direction respectively.

Consider a ray $\mathbf{r}(t) = \mathbf{o} + t\mathbf{d}$ with the ray origin $\mathbf{o} \in \mathbb{R}^3$, let us denote $\sigma(t)$ and $\mathbf{c}(t)$ as the density and color at point $\mathbf{r}(t)$ respectively. NeRF renders the expected color $\mathbf{C}(\mathbf{r})$ by using alpha composition of densities and colors along the ray which is approximated by numerical quadrature [69] as follows:

$$\begin{aligned} \mathbf{C}(\mathbf{r}) &= \sum_{k=1}^K T(t_k) \alpha(t_k) \mathbf{c}(t_k), \\ \text{where } \alpha(t_k) &= 1 - \exp(-\sigma(t_k) \delta_k), \\ T(t_k) &= \prod_{k'=1}^{k-1} (1 - \alpha(t_{k'})) \\ &= \exp\left(-\sum_{k'=1}^{k-1} \sigma(t_{k'}) \delta_{k'}\right), \end{aligned} \quad (2)$$

where $\{t_k\}_{k=1}^K$ is a set of sampled points, selected by using stratified sampling for volume rendering, and $\delta_k = t_{k+1} - t_k$ refers to the distance between the adjacent sampled points.

To increase sampling efficiency, NeRF simultaneously trains two MLPs that share the same structure: ‘‘Coarse’’ and ‘‘fine’’ networks where the coarse network determines the sampling points to feed into the fine network.

Latent Conditional NeRF. To synthesize views from photographs with variable illumination, previous methods [28, 28–30] have mainly used appearance embedding $\ell_i^{(a)} \in \mathbb{R}^{n^{(a)}}$ which grants NeRF the flexibility to adjust the emitted radiance of the scene for each image \mathcal{I}_i . The radiance \mathbf{c} in Eq. (1) and rendered color $\mathbf{C}(\mathbf{r})$ in Eq. (2) are replaced with image-dependent \mathbf{c}_i and $\mathbf{C}_i(\mathbf{r})$ as follows:

$$\begin{aligned} \mathbf{c}_i &= \text{MLP}_{\theta_2}(\gamma_{\mathbf{d}}(\mathbf{d}), \mathbf{z}, \ell_i^{(a)}), \\ \mathbf{C}_i(\mathbf{r}) &= \sum_{k=1}^K T(t_k) \alpha(t_k) \mathbf{c}_i(t_k). \end{aligned} \quad (3)$$

Following the framework of NeRF-W [28, 70], we adopt the appearance embeddings, optimizing them for each input image.

Mip-NeRF. Instead of casting a single ray for each pixel like NeRF, mip-NeRF [3] casts a cone of which the radius changes as the resolution of the image changes. Mip-NeRF changes the positional encoding scheme from encoding an infinitesimally small point to integrating within the conical frustum (Integrated Positional Encoding) for each section of the ray. This enables mip-NeRF to learn multiscale representations and thereby combine NeRF’s coarse and fine MLPs into a single MLP. We follow the mip-NeRF structure

in this work to take advantage of the halved model capacity and scale robustness since in-the-wild photographs are taken at varying camera distances and resolutions.

3.2. Semantic-aware Scene Decomposition

To achieve consistent scene decomposition, we use an additional MLP module, dubbed FilterNet, that models transient components by leveraging semantic features of the images. FilterNet T_ψ is designed to handle transient phenomena by learning image-dependent 2D maps: transient RGBA and uncertainty maps. The transient RGBA image is alpha blended with the rendered (static) image produced by NeRF to reconstruct the original image as shown in Figure 1. We estimate the uncertainty of the observed color for each pixel, enabling the model to adjust its reconstruction loss by disregarding unreliable pixels. This idea is borrowed from NeRF-W [28], but the difference is that we directly estimate a 2D uncertainty map, while NeRF-W renders the value with uncertainties of 3D locations along the ray.

To be specific, we model FilterNet T_ψ as an implicit continuous function that maps a transient embedding $\ell_i^{(\tau)} \in \mathbb{R}^{n^{(\tau)}}$, a pixel location $\mathbf{p} \in \mathbb{R}^2$ and its corresponding encoded feature $\mathbf{f}_i(\mathbf{p}) \in \mathbb{R}^F$ to transient color $\mathbf{C}_i^{(\tau)}$, opacity $\alpha_i^{(\tau)} \in [0, 1]$ and uncertainty $\beta_i \in \mathbb{R}^+$ values as:

$$\left[\alpha_i^{(\tau)}, \mathbf{C}_i^{(\tau)}, \beta_i\right] = T_\psi\left(\gamma_{\mathbf{p}}(\mathbf{p}), \ell_i^{(\tau)}, \mathbf{f}_i(\mathbf{p})\right), \quad (4)$$

where $\gamma_{\mathbf{p}} : \mathbb{R}^2 \rightarrow \mathbb{R}^{4L}$ is the positional encoding function applied to each pixel coordinate. Feature map \mathbf{f}_i is extracted from input image \mathcal{I}_i with the encoder $E : \mathbb{R}^{H \times W \times 3} \rightarrow \mathbb{R}^{H \times W \times F}$ that can be pre-trained on other real-world datasets.

Let us denote $\mathbf{C}_i^{(\tau)}(\mathbf{p}_{\mathbf{r}})$, $\alpha_i^{(\tau)}(\mathbf{p}_{\mathbf{r}})$ and $\beta_i(\mathbf{p}_{\mathbf{r}})$ as the transient color, opacity and uncertainty values of a pixel corresponding to ray \mathbf{r} , respectively. The final predicted pixel color $\hat{\mathbf{C}}_i(\mathbf{r})$ is then obtained by combining transient color $\mathbf{C}_i^{(\tau)}(\mathbf{p}_{\mathbf{r}})$ and static color $\mathbf{C}_i(\mathbf{r})$ with alpha blending as follows:

$$\hat{\mathbf{C}}_i(\mathbf{r}) = \alpha_i^{(\tau)}(\mathbf{p}_{\mathbf{r}}) \mathbf{C}_i^{(\tau)}(\mathbf{p}_{\mathbf{r}}) + (1 - \alpha_i^{(\tau)}(\mathbf{p}_{\mathbf{r}})) \mathbf{C}_i(\mathbf{r}). \quad (5)$$

For each ray \mathbf{r} in image \mathcal{I}_i , we train FilterNet to disentangle transient components from the scene in an unsupervised manner with loss $\mathcal{L}_i^{(i)}$:

$$\mathcal{L}_i^{(i)}(\mathbf{r}) = \frac{\|\hat{\mathbf{C}}_i(\mathbf{r}) - \bar{\mathbf{C}}_i(\mathbf{r})\|_2^2}{2\beta_i(\mathbf{p}_{\mathbf{r}})^2} + \frac{\log \beta_i(\mathbf{p}_{\mathbf{r}})^2}{2} + \lambda_\alpha \alpha_i^{(\tau)}(\mathbf{p}_{\mathbf{r}}), \quad (6)$$

where $\bar{\mathbf{C}}$ is the ground-truth color. The first and second terms can be viewed as the negative log-likelihood of $\hat{\mathbf{C}}_i(\mathbf{r})$ which is assumed to follow an isotropic normal distribution with mean $\bar{\mathbf{C}}_i(\mathbf{r})$ and variance $\beta_i(\mathbf{p}_{\mathbf{r}})^2$ [28]. The third term discourages FilterNet from describing static phenomena.

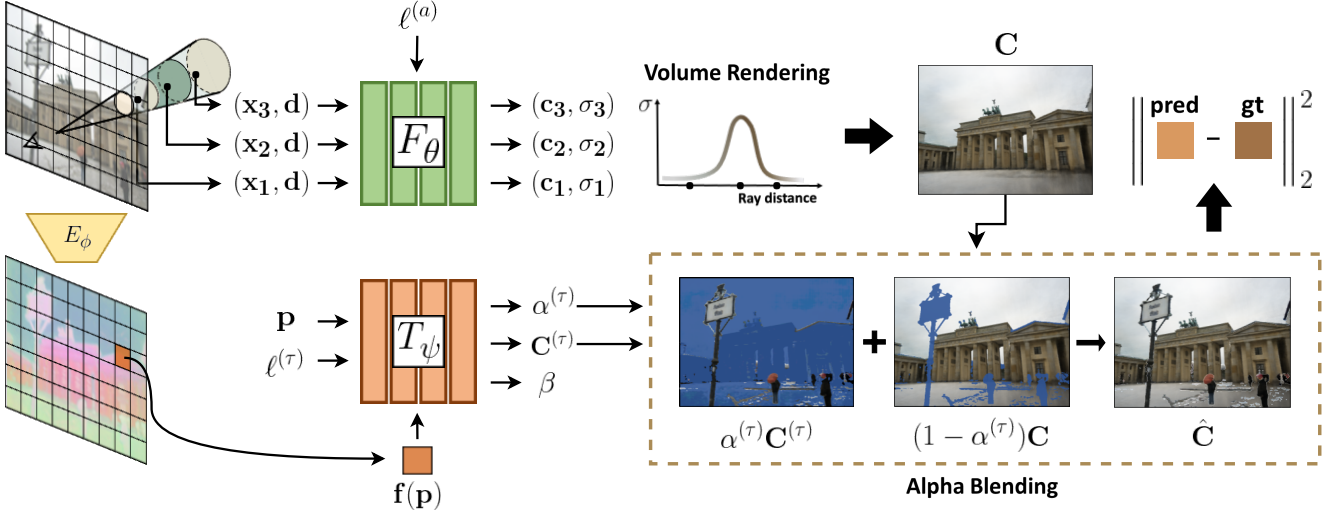


Figure 1. **Overall architecture.** Our framework decomposes the scene into static and transient components by filtering out transient occluders in the image. Given a 3D position \mathbf{x} , direction \mathbf{d} and learned appearance embedding $\ell^{(a)}$, the static NeRF model F_θ produces static color and density, which are used to render static images. For each image, FilterNet T_ψ maps pixel location \mathbf{p} to its transient opacity $\alpha^{(\tau)}$, transient color $\mathbf{C}^{(\tau)}$ and uncertainty value β conditioned on an image-dependent transient embedding $\ell^{(\tau)}$ and pixel-wise feature $\mathbf{f}(\mathbf{p})$ extracted from the image encoder E_ϕ . The final predicted pixel color $\hat{\mathbf{C}}$ is then calculated by alpha blending rendered static color \mathbf{C} and transient color $\mathbf{C}^{(\tau)}$.

3.3. Transient Opacity Reparameterization

We empirically found that a naive adoption of FilterNet yields ambiguous transient opacity values, *i.e.*, values that are not close to zero or one, if trained to predict them by simply passing the output of the MLP through a sigmoid activation function. This ambiguous decomposition leads to blurry artifacts in the static scene.

We encourage transient images to be either fully opaque or empty by modeling $\alpha_i^{(\tau)}$ as a Binary Concrete random variable [71], which is a continuous relaxation of Bernoulli random variable, and predicting its probability. Binary Concrete distribution is a special case of Concrete distribution, also known as Gumbel-Softmax distribution [72], which is usually used to approximate discrete random variables.

We sample $\alpha_i^{(\tau)}$ from a Binary Concrete distribution with location parameter $\tilde{\alpha}_i \in (0, \infty)$, which our FilterNet will predict instead of directly predicting the opacity value as follows:

$$\alpha_i^{(\tau)} = \text{sigmoid}\left(\frac{1}{t} \cdot (\log \tilde{\alpha}_i + \log U - \log(1 - U))\right), \quad (7)$$

$$U \sim \text{Uniform}(0, 1), \quad (8)$$

where $t \in (0, \infty)$ is a hyperparameter. This sampling scheme encourages our model to predict opacity values concentrated on the boundaries of the interval $[0, 1]$, while allowing backpropagation. During evaluation, we fix U to 0.5.

3.4. Transient Opacity Smoothness Prior

The inputs of Filternet: encoded pixel (PE features) $\gamma_{\mathbf{p}}(\mathbf{p})$, image feature $\mathbf{f}(\mathbf{p})$, and embedding $\ell^{(\tau)}$, contain high-frequency information. This naturally leads to high-frequency outputs which is suitable for predicting the color of a pixel, but could cause noisy prediction of transient opacity. We thus add a smoothness loss on the transient opacity field as:

$$\mathcal{L}_{\text{sm}}^{(i)}(\mathbf{p}) = \sum_{k=0}^{L-1} 2^k \left\| \frac{\partial \alpha_i^{(\tau)}(\mathbf{p})}{\partial \gamma_k(\mathbf{p})} \right\|_1, \quad (9)$$

where $\gamma_k(\mathbf{p}) = [\cos(2^k \pi \mathbf{p}), \sin(2^k \pi \mathbf{p})]$ is the k -th frequency encoding of \mathbf{p} . The loss term multiplied by a constant value is the upper bound of L1-norm of the derivative of $\alpha_i^{(\tau)}$ with respect to the pixel coordinate, *i.e.*, $\left\| \frac{\partial \alpha_i^{(\tau)}(\mathbf{p})}{\partial \mathbf{p}} \right\|_1 \leq \sum_{k=0}^{L-1} 2^k \pi \left\| \frac{\partial \alpha_i^{(\tau)}(\mathbf{p})}{\partial \gamma_k(\mathbf{p})} \right\|_1$, which essentially enforces smoothness on transient opacity field. We have taken this indirect approach to reduce the sensitivity of our model to the regularization term. The inequality above can be simply derived by using chain rule and triangle inequality.

3.5. Optimization

We jointly optimize the model parameters (θ, ϕ, ψ) , the per-image appearance embeddings $\{\ell_i^{(a)}\}_{i=1}^N$ and the tran-

sient embeddings $\{\ell_i^{(\tau)}\}_{i=1}^N$ by minimizing the total loss:

$$\sum_{i=1}^N \sum_{\mathbf{r} \in \mathcal{R}_i} [\mathcal{L}_t^{(i)}(\mathbf{r}) + \lambda_c \mathcal{L}_c^{(i)}(\mathbf{r}) + \lambda_{sm} \mathcal{L}_{sm}^{(i)}(\mathbf{p}_r) + \lambda_{sp} \mathcal{L}_{sp}(\mathbf{r})] + \lambda_a \|\ell_i^{(a)}\|_2^2, \quad (10)$$

where $\lambda_c, \lambda_{sm}, \lambda_{sp}$ and λ_a are the hyperparameters and $\mathcal{L}_c^{(i)}$ is the reconstruction loss of rendered images composited with coarse samples $\mathbf{t}^c = \{t_k^c\}_{k=1}^K$, and \mathcal{L}_{sp} is a regularization term named sparsity loss:

$$\mathcal{L}_c^{(i)}(\mathbf{r}) = \left(1 - \alpha_i^{(\tau)}(\mathbf{p}_r)\right) \|\mathbf{C}_i(\mathbf{r}; \mathbf{t}^c) - \bar{\mathbf{C}}_i(\mathbf{r})\|_2^2, \quad (11)$$

$$\mathcal{L}_{sp}(\mathbf{r}) = \sum_k \log(1 + 2\sigma(t_k^c)^2), \quad (12)$$

where $\mathbf{t}^c = \{t_k^c\}_{k=1}^K$ are the coarse samples produced with stratified sampling.

Sparsity loss \mathcal{L}_{sp} encourages the static scene to have zero density on the unobserved areas. Since transient objects hide the static scene, the static model cannot learn the scene representation on those areas. When sufficient training images are given, this obstruction is negligible since other images provide the chance to observe the missing area. However, in the few-shot setting, this cannot be guaranteed and allows the model to freely generate arbitrary geometry in the unobserved regions. We hence use this sparsity prior which is also known as Cauchy loss [5, 73] to encourage the sparsity of NeRF’s opacity field.

4. Experiments

In this section, we show that our method, referred to as SF-NeRF, outperforms the previous state-of-the-art approach both quantitatively and qualitatively. Then we provide extensive ablation studies and visualizations to validate the effectiveness of the components in SF-NeRF.

Datasets. We demonstrate our approach on four training sets which consist of internet photo collections of cultural landmarks from the Phototourism dataset [32]: “Brandenburg Gate”, “Sacre Coeur”, “Trevi Fountain” and “Taj Mahal”. We follow the split used by HA-NeRF [31] and down-sample the images by 2 times as HA-NeRF did. For each landmark, we evaluate our method under the few-shot settings, sampling 15 and 30 images out of 700~1700 images.

Baselines. We compare our method to NeRF [1], NeRF-W [28], HA-NeRF [31] and one variant of NeRF-W which we call as NeRF-AM. NeRF-AM shares the same structure as NeRF-W with its transient head eliminated (a.k.a., NeRF-A) and eliminates transient objects using a pre-trained semantic segmentation model. NeRF-AM uses DeepLabv3+ [74] trained on Cityscapes dataset [75] and masks out movable objects such as people (person, rider)

and vehicles (rider, car, truck, bus, train, motorcycle, bicycle). For a fair comparison, all models share the same static NeRF model architecture which consists of 8 layers of 256 hidden units for generating density σ and one additional layer of 128 hidden units for color \mathbf{c} .

Implementation details. For the image encoder E_ϕ , we use DINO [76] model, a pretrained self-supervised 2D image feature extractor, followed by 3 fully connected layers of 128 hidden units. Since the feature map extracted by DINO is reduced in size, we first resize them to the original image size and then pass through the MLP layers. In the few-shot setting, the encoder is first pre-trained on full images of “Temple Nara Japan” in Phototourism to learn the prior of transient objects. FilterNet T_ψ consists of 5 fully connected layers of 128 hidden units, with a sigmoid and two softplus activation functions for $\mathbf{c}_i^{(\tau)}$, β_i and $\tilde{\alpha}_i$ respectively. For each β_i , we add $\beta_{\min} = 0.1$ to assign minimum importance to each ray. Each appearance and transient embedding has an embedding dimension of size $n^{(a)} = 48$ and $n^{(\tau)} = 128$.

Evaluation All methods are evaluated on the task of novel view synthesis. We report the standard image quality metrics, Peak Signal to Noise Ratio (PSNR), Structural Similarity Index Measure (SSIM) [77], and Learned Perceptual Image Patch Similarity (LPIPS) [78] with AlexNet for all evaluations. Since the appearance embeddings are only optimized for training set images, a procedure to obtain appearance embeddings for each test image is essential. We evaluate each baseline following their evaluation scheme, where NeRF-W optimizes the embedding on the left half of each test image and reports metrics on the right half, and HA-NeRF obtains the appearance embedding by its learned encoder. Here we evaluate our approach using the scheme of NeRF-W.

4.1. Results

The overall quantitative results are shown in Table 1, where SF-NeRF mostly outperforms the baselines in the few-shot setting. While SF-NeRF overall improves performance, the gap is not dramatic. This is explainable if we look at the test set of Phototourism dataset. As shown in Figure 5, most of the test images contain only the visible part, *i.e.*, the parts that were not hidden by the transient occluders, of the landmark during training. Therefore, evaluating these images may not reflect the ability to decompose static and transient components. Though the qualitative results show a clear improvement in SF-NeRF over the baselines.

Figure 2 shows the qualitative results of our model and the baselines on some examples of the dataset. Rendering with NeRF often results in global color shifts and ghosting



Figure 2. **Qualitative Results** of novel view synthesis on Phototourism dataset [32] under the few-shot setting (30 images). SF-NeRF learns the separated static scene well while other baselines remain ghosting/blurry artifacts.

Few15	Brandenburg Gate			Sacre Coeur			Trevi Fountain			Taj Mahal		
	PSNR	SSIM	LPIPS	PSNR	SSIM	LPIPS	PSNR	SSIM	LPIPS	PSNR	SSIM	LPIPS
NeRF [1]	11.54	0.536	0.503	13.25	0.581	0.409	12.36	0.415	0.474	11.99	0.564	0.506
NeRF-AM	13.65	0.627	0.468	17.53	0.675	0.290	17.53	0.538	0.351	19.21	0.733	0.313
NeRF-W [28]	20.80	0.787	0.266	17.87	0.715	0.235	18.15	0.596	0.333	20.32	0.787	0.259
HA-NeRF [31]	13.83	0.693	0.516	15.41	0.675	0.423	14.60	0.540	0.416	13.84	0.703	0.458
SF-NeRF	19.72	0.790	0.260	17.69	0.707	0.240	18.94	0.607	0.281	20.47	0.801	0.226
Few30	Brandenburg Gate			Sacre Coeur			Trevi Fountain			Taj Mahal		
	PSNR	SSIM	LPIPS	PSNR	SSIM	LPIPS	PSNR	SSIM	LPIPS	PSNR	SSIM	LPIPS
NeRF [1]	11.42	0.514	0.488	10.04	0.421	0.551	11.31	0.333	0.496	11.28	0.490	0.588
NeRF-AM	13.20	0.628	0.434	12.94	0.506	0.531	15.44	0.441	0.445	18.41	0.686	0.338
NeRF-W [28]	22.74	0.847	0.188	19.31	0.750	0.205	19.54	0.646	0.298	21.03	0.792	0.259
HA-NeRF [31]	19.88	0.803	0.278	17.66	0.736	0.256	16.97	0.598	0.352	17.92	0.785	0.321
SF-NeRF	23.23	0.846	0.178	19.64	0.757	0.186	20.24	0.657	0.243	20.86	0.820	0.208

Table 1. Quantitative results of experiments on Phototourism dataset [32] in the few-shot settings (15/30 images). We report PSNR/SSIM (higher is better) and LPIPS (lower is better). SF-NeRF mostly outperforms the baselines in the few-shot setting.

artifacts. These are the direct consequences of the assumption of NeRF we’ve explained in Section 1 that the scene is

constant across all images and every content in the scene is static. While NeRF-AM, HA-NeRF, and NeRF-W are able

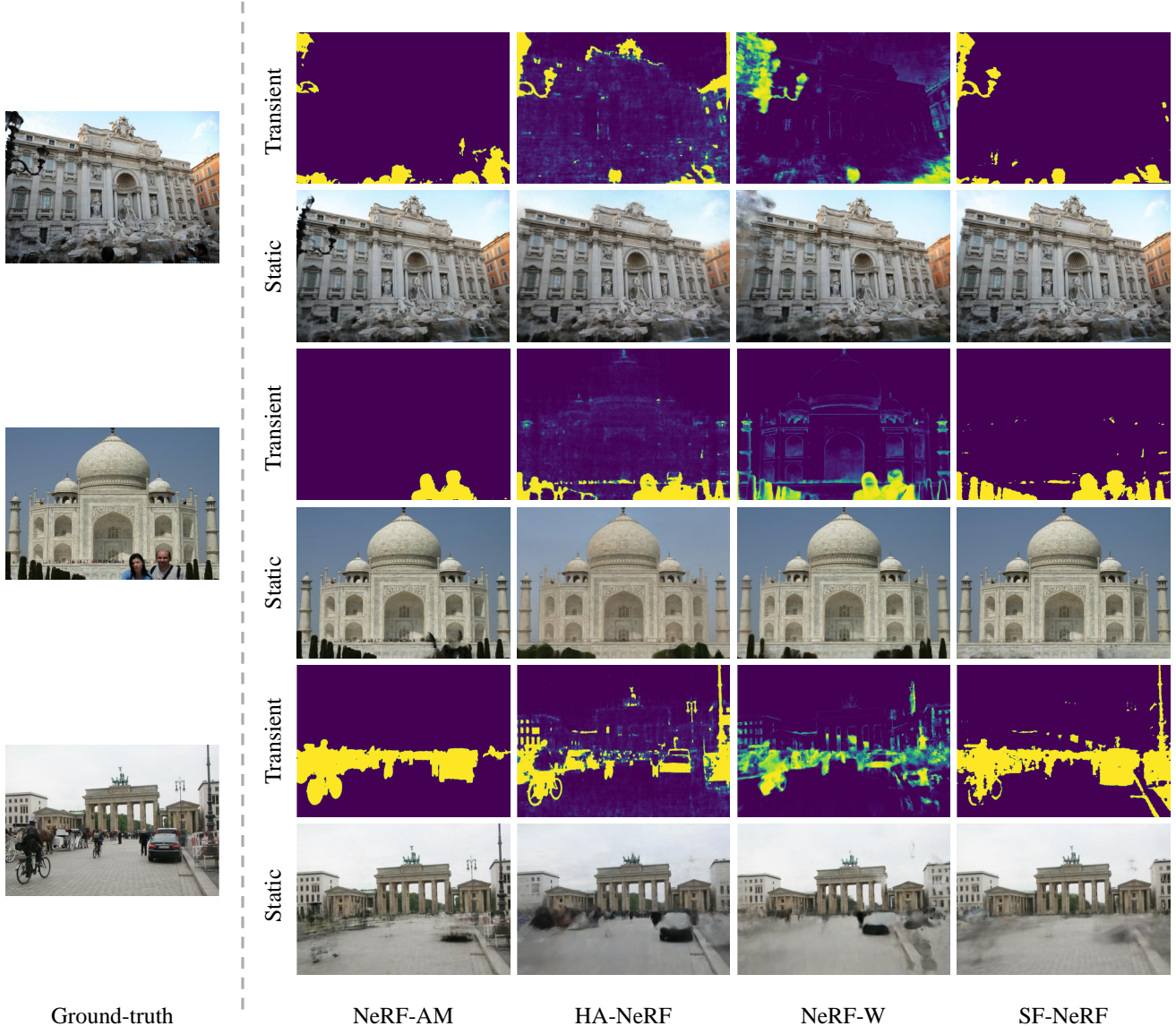


Figure 3. **Predicted transient opacity/visibility maps (Transient) and rendered static images (Static)** of SF-NeRF and other baselines. The predicted transient opacity map of NeRF-AM is based on the result of pretrained segmentation model, HA-NeRF directly learns an image-wise 2D visibility map and that of NeRF-W is rendered with the 3D transient field of NeRF-W.

	PSNR \uparrow	SSIM \uparrow	LPIPS \downarrow
w/o Concrete	20.65	0.823	0.248
w/o Smooth	22.27	0.802	0.191
SF-NeRF	23.23	0.846	0.178

Table 2. Ablation study of transient opacity reparameterization (Concrete) and smoothness prior (Smooth) on “Brandenburg Gate” dataset in the few-shot setting (30 images).

to model varying photometric effects thanks to the usage of appearance embeddings, they also suffer from artifacts. Specifically, the three baselines show ghosting artifacts in “Taj Mahal” and “Brandenburg Gate” (especially on NeRF-AM) and blurry artifacts in “Trevi Fountain”. It can be seen that most of the artifacts are placed on the area that are often hidden from the transient occluders, which indicates that they lack the ability to decompose static and transient components. This observation is supported by Figure 3 where NeRF-AM, HA-NeRF and NeRF-W often miss to remove some of the transient objects. On the contrary, SF-NeRF

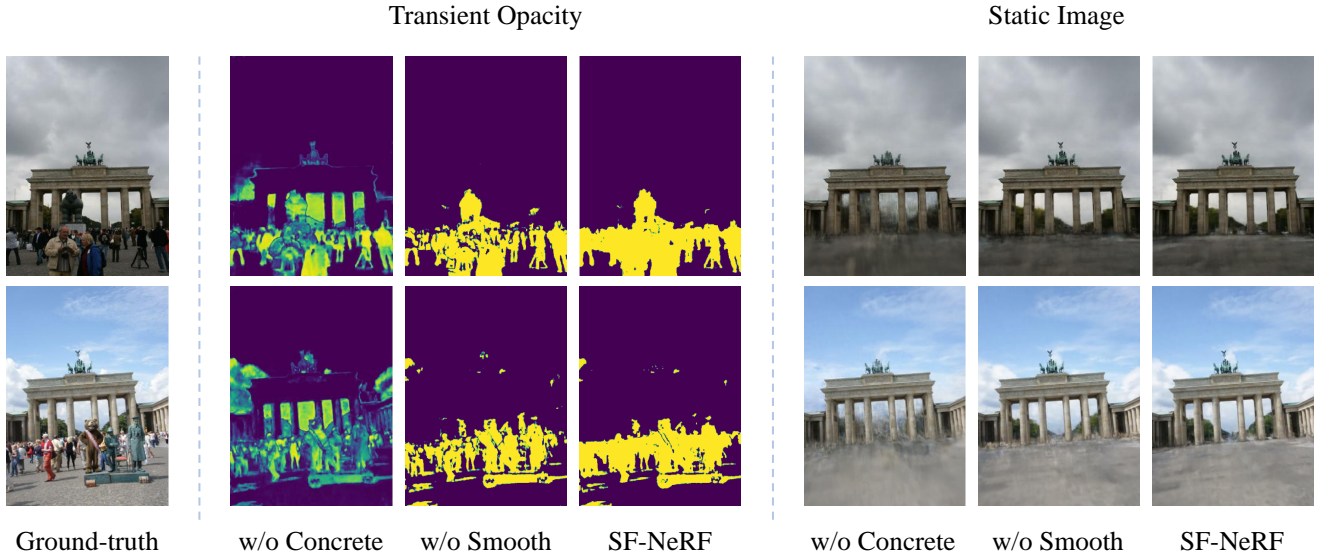


Figure 4. **Qualitative ablation results** on “Brandenburg Gate” dataset where we compare our method with two other ablations of SF-NeRF: without transient opacity reparameterization (Concrete) or transient opacity smoothness prior (Smooth).



Figure 5. **Examples of training and test images from Photo-tourism dataset** [32]. The high part of the landmark, where the transient occluders can be hardly placed, occupies a large part of the test images.

consistently disentangles transient elements from the static scene which proves the effectiveness of the semantic-guided filtering module.

4.2. Ablations Studies

We conduct ablation studies to analyze the individual contribution of each component in the proposed method. “w/o Concrete” removes the transient opacity reparameterization trick and replaces the activation of $\tilde{\alpha}_i$ from softplus to sigmoid, and “w/o Smooth” removes the transient opacity smoothness regularization term $\mathcal{L}_{sm}^{(i)}$. We evaluate on the “Brandenburg Gate” dataset and provide the results in Ta-

ble 2 and Figure 4.

As shown in Table 2, using all the components (Concrete reparameterization and smoothness prior) achieves considerable improvement compared to the ablations of SF-NeRF: improves by on average 2.6dB and 1.0dB in PSNR compared to “w/o Concrete” and “w/o Smooth” respectively. Figure 4 shows qualitative ablation results on the two components. As mentioned in Section 3.3, if the Concrete reparameterization trick is removed (“w/o Concrete”), FilterNet yields ambiguous transient opacity values which leads to blurry, ghosting artifacts. In the case of the transient opacity smoothness prior, “w/o Smooth” predicts noisy transient opacity, in other words, the opacities are sparsely predicted. The missing part of the opacities may also cause such artifacts, which is shown in Figure 4.

4.3. Limitations and Future Work

SF-NeRF solely focus on removing the transient phenomena well in the way of solving the few-shot novel view synthesis from the in-the-wild photographs. In order to improve further, approach to learn the geometry and varying appearance of the static scene well in the few-shot setting is necessary. Furthermore, the camera parameters for each image which are obtained by using structure-from-motion [79] are not entirely accurate. Since we train with few images, SF-NeRF is sensitive to camera calibration errors and this leads to blurry reconstructions. Therefore, simultaneously performing camera pose refinement could be one solution.

5. Conclusion

We propose a novel learning framework to learn neural representations from a small number of in-the-wild photographs, named as “Semantic-aware Occlusion Filtering Neural Radiance Fields (SF-NeRF)”. SF-NeRF focus on decomposing the transient and static phenomena, predicting the transient components of each image with an additional MLP module dubbed FilterNet. FilterNet exploits semantic information given by an image encoder pretrained in an unsupervised manner, which is the key to achieve few-shot learning. Moreover, we apply a reparameterization technique to prevent ambiguous decomposition and employ a smoothness prior on the transient opacity. We show that SF-NeRF overall outperforms state-of-the-art novel view synthesis methods on Phototourism dataset under the few-shot setting.

References

- [1] Ben Mildenhall, Pratul P. Srinivasan, Matthew Tancik, Jonathan T. Barron, Ravi Ramamoorthi, and Ren Ng. Nerf: Representing scenes as neural radiance fields for view synthesis. In *ECCV*, 2020. 1, 2, 5, 6
- [2] Thomas Müller, Alex Evans, Christoph Schied, and Alexander Keller. Instant neural graphics primitives with a multiresolution hash encoding. *ACM Trans. Graph.*, 2022. 1, 2
- [3] Jonathan T. Barron, Ben Mildenhall, Matthew Tancik, Peter Hedman, Ricardo Martin-Brualla, and Pratul P. Srinivasan. Mip-nerf: A multiscale representation for anti-aliasing neural radiance fields. In *ICCV*, 2021. 1, 2, 3
- [4] Alex Yu, Ruilong Li, Matthew Tancik, Hao Li, Ren Ng, and Angjoo Kanazawa. PlenOctrees for real-time rendering of neural radiance fields. In *ICCV*, 2021. 1, 2
- [5] Sara Fridovich-Keil and Alex Yu, Matthew Tancik, Qinhong Chen, Benjamin Recht, and Angjoo Kanazawa. Plenoxels: Radiance fields without neural networks. In *CVPR*, 2022. 1, 2, 5
- [6] Stephan J. Garbin, Marek Kowalski, Matthew Johnson, Jamie Shotton, and Julien Valentin. Fastnerf: High-fidelity neural rendering at 200fps. In *ICCV*, 2021. 1, 2
- [7] Christian Reiser, Songyou Peng, Yiyi Liao, and Andreas Geiger. Kilonerf: Speeding up neural radiance fields with thousands of tiny mlps. In *ICCV*, 2021. 1, 2
- [8] Liangchen Song, Anpei Chen, Zhong Li, Zhang Chen, Lele Chen, Junsong Yuan, Yi Xu, and Andreas Geiger. Nerfplayer: A streamable dynamic scene representation with decomposed neural radiance fields. *arXiv preprint arXiv:2210.15947*, 2022. 1, 2
- [9] Albert Pumarola, Enric Corona, Gerard Pons-Moll, and Francesc Moreno-Noguer. D-nerf: Neural radiance fields for dynamic scenes. In *CVPR*, 2021. 1, 2
- [10] Keunhong Park, Utkarsh Sinha, Jonathan T. Barron, Sofien Bouaziz, Dan B Goldman, Steven M. Seitz, and Ricardo Martin-Brualla. Nerfies: Deformable neural radiance fields. In *ICCV*, 2021. 1, 2
- [11] Keunhong Park, Utkarsh Sinha, Peter Hedman, Jonathan T Barron, Sofien Bouaziz, Dan B Goldman, Ricardo Martin-Brualla, and Steven M Seitz. Hypernerf: A higher-dimensional representation for topologically varying neural radiance fields. *arXiv preprint arXiv:2106.13228*, 2021. 1, 2
- [12] Chen Gao, Ayush Saraf, Johannes Kopf, and Jia-Bin Huang. Dynamic view synthesis from dynamic monocular video. In *ICCV*, pages 5712–5721, 2021. 1, 2
- [13] Zhengqi Li, Simon Niklaus, Noah Snavely, and Oliver Wang. Neural scene flow fields for space-time view synthesis of dynamic scenes. In *CVPR*, 2021. 1, 2
- [14] Edgar Tretschk, Ayush Tewari, Vladislav Golyanik, Michael Zollhöfer, Christoph Lassner, and Christian Theobalt. Non-rigid neural radiance fields: Reconstruction and novel view synthesis of a dynamic scene from monocular video. In *ICCV*, 2021. 1, 2
- [15] Yilun Du, Yinan Zhang, Hong-Xing Yu, Joshua B Tenenbaum, and Jiajun Wu. Neural radiance flow for 4d view synthesis and video processing. In *ICCV*, 2021. 1, 2
- [16] Wentao Yuan, Zhaoyang Lv, Tanner Schmidt, and Steven Lovegrove. Star: Self-supervised tracking and reconstruction of rigid objects in motion with neural rendering. In *CVPR*, 2021. 1, 2
- [17] Mijeong Kim, Seonguk Seo, and Bohyung Han. Infonerf: Ray entropy minimization for few-shot neural volume rendering. In *CVPR*, 2022. 1, 2
- [18] Alex Yu, Vickie Ye, Matthew Tancik, and Angjoo Kanazawa. pixelNeRF: Neural radiance fields from one or few images. In *CVPR*, 2021. 1, 2
- [19] Dejia Xu, Yifan Jiang, Peihao Wang, Zhiwen Fan, Humphrey Shi, and Zhangyang Wang. Sinnerf: Training neural radiance fields on complex scenes from a single image. In *ECCV*, 2022. 1
- [20] Ajay Jain, Matthew Tancik, and Pieter Abbeel. Putting nerf on a diet: Semantically consistent few-shot view synthesis. In *ICCV*, 2021. 1, 2
- [21] Michael Niemeyer, Jonathan T. Barron, Ben Mildenhall, Mehdi S. M. Sajjadi, Andreas Geiger, and Noha Radwan. Regnerf: Regularizing neural radiance fields for view synthesis from sparse inputs. In *CVPR*, 2022. 1, 2
- [22] Norman Müller, Andrea Simonelli, Lorenzo Porzi, Samuel Rota Bulò, Matthias Nießner, and Peter Kotschieder. Autorf: Learning 3d object radiance fields from single view observations. In *CVPR*, 2022. 1, 2
- [23] Yuan Liu, Sida Peng, Lingjie Liu, Qianqian Wang, Peng Wang, Christian Theobalt, Xiaowei Zhou, and Wenping Wang. Neural rays for occlusion-aware image-based rendering. In *CVPR*, 2022. 1, 2
- [24] Konstantinos Rematas, Ricardo Martin-Brualla, and Vittorio Ferrari. Sharf: Shape-conditioned radiance fields from a single view. *ICML*, 2021. 1

- [25] Qianqian Wang, Zhicheng Wang, Kyle Genova, Pratul P Srinivasan, Howard Zhou, Jonathan T Barron, Ricardo Martin-Brualla, Noah Snavely, and Thomas Funkhouser. Ibrnet: Learning multi-view image-based rendering. In *CVPR*, 2021. 1, 2
- [26] Yi Wei, Shaohui Liu, Yongming Rao, Wang Zhao, Jiwen Lu, and Jie Zhou. Nerfingmvs: Guided optimization of neural radiance fields for indoor multi-view stereo. In *ICCV*, 2021. 1
- [27] Mohammad Mahdi Johari, Yann Lepoittevin, and François Fleuret. Geonerf: Generalizing nerf with geometry priors. In *CVPR*, 2022. 1, 2
- [28] Ricardo Martin-Brualla, Noha Radwan, Mehdi S. M. Sajjadi, Jonathan T. Barron, Alexey Dosovitskiy, and Daniel Duckworth. NeRF in the Wild: Neural Radiance Fields for Unconstrained Photo Collections. In *CVPR*, 2021. 1, 2, 3, 5, 6
- [29] Matthew Tancik, Vincent Casser, Xincheng Yan, Sabeek Pradhan, Ben Mildenhall, Pratul P Srinivasan, Jonathan T Barron, and Henrik Kretzschmar. Block-nerf: Scalable large scene neural view synthesis. In *CVPR*, 2022. 1, 2, 3
- [30] Haithem Turki, Deva Ramanan, and Mahadev Satyanarayanan. Mega-nerf: Scalable construction of large-scale nerfs for virtual fly-throughs. In *CVPR*, 2022. 1, 2, 3
- [31] Xingyu Chen, Qi Zhang, Xiaoyu Li, Yue Chen, Ying Feng, Xuan Wang, and Jue Wang. Hallucinated neural radiance fields in the wild. In *CVPR*, 2022. 1, 2, 5, 6
- [32] Yuhe Jin, Dmytro Mishkin, Anastasiia Mishchuk, Jiri Matas, Pascal Fua, Kwang Moo Yi, and Eduard Trulls. Image matching across wide baselines: From paper to practice. *International Journal of Computer Vision*, 2021. 1, 2, 5, 6, 8
- [33] Sai Bi, Zexiang Xu, Kalyan Sunkavalli, Miloš Hašan, Yannick Hold-Geoffroy, David Kriegman, and Ravi Ramamoorthi. Deep reflectance volumes: Relightable reconstructions from multi-view photometric images. In *ECCV*, 2020. 2
- [34] Stephen Lombardi, Tomas Simon, Jason Saragih, Gabriel Schwartz, Andreas Lehrmann, and Yaser Sheikh. Neural volumes: Learning dynamic renderable volumes from images. *arXiv preprint arXiv:1906.07751*, 2019. 2
- [35] Justus Thies, Michael Zollhöfer, and Matthias Nießner. Deferred neural rendering: Image synthesis using neural textures. *ACM Trans. Graph.*, 2019. 2
- [36] Tinghui Zhou, Richard Tucker, John Flynn, Graham Fyffe, and Noah Snavely. Stereo magnification: Learning view synthesis using multiplane images. *arXiv preprint arXiv:1805.09817*, 2018. 2
- [37] Vincent Sitzmann, Justus Thies, Felix Heide, Matthias Nießner, Gordon Wetzstein, and Michael Zollhofer. Deepvoxels: Learning persistent 3d feature embeddings. In *CVPR*, 2019. 2
- [38] Peng Dai, Yinda Zhang, Zhuwen Li, Shuaicheng Liu, and Bing Zeng. Neural point cloud rendering via multi-plane projection. In *CVPR*, 2020. 2
- [39] Lars Mescheder, Michael Oechsle, Michael Niemeyer, Sebastian Nowozin, and Andreas Geiger. Occupancy networks: Learning 3d reconstruction in function space. In *CVPR*, 2019. 2
- [40] Jeong Joon Park, Peter Florence, Julian Straub, Richard Newcombe, and Steven Lovegrove. DeepSDF: Learning continuous signed distance functions for shape representation. In *CVPR*, 2019. 2
- [41] Ben Mildenhall, Peter Hedman, Ricardo Martin-Brualla, Pratul P Srinivasan, and Jonathan T Barron. Nerf in the dark: High dynamic range view synthesis from noisy raw images. In *CVPR*, 2022. 2
- [42] Dor Verbin, Peter Hedman, Ben Mildenhall, Todd Zickler, Jonathan T Barron, and Pratul P Srinivasan. Ref-nerf: structured view-dependent appearance for neural radiance fields. In *CVPR*, 2022. 2
- [43] Katja Schwarz, Yiyi Liao, Michael Niemeyer, and Andreas Geiger. Graf: Generative radiance fields for 3d-aware image synthesis. In *CVPR*, 2021. 2
- [44] Michael Niemeyer and Andreas Geiger. Giraffe: Representing scenes as compositional generative neural feature fields. In *CVPR*, 2021. 2
- [45] Ajay Jain, Ben Mildenhall, Jonathan T. Barron, Pieter Abbeel, and Ben Poole. Zero-shot text-guided object generation with dream fields. In *CVPR*, 2022. 2
- [46] Ben Poole, Ajay Jain, Jonathan T. Barron, and Ben Mildenhall. Dreamfusion: Text-to-3d using 2d diffusion. *arXiv preprint arXiv:2209.14988*, 2022. 2
- [47] Eric R Chan, Marco Monteiro, Petr Kellnhofer, Jiajun Wu, and Gordon Wetzstein. pi-gan: Periodic implicit generative adversarial networks for 3d-aware image synthesis. In *CVPR*, 2021. 2
- [48] Lingjie Liu, Jiatao Gu, Kyaw Zaw Lin, Tat-Seng Chua, and Christian Theobalt. Neural sparse voxel fields. *NeurIPS*, 2020. 2
- [49] Anpei Chen, Zexiang Xu, Fuqiang Zhao, Xiaoshuai Zhang, Fanbo Xiang, Jingyi Yu, and Hao Su. Mvsnerf: Fast generalizable radiance field reconstruction from multi-view stereo. In *ICCV*, 2021. 2
- [50] Zirui Wang, Shangzhe Wu, Weidi Xie, Min Chen, and Victor Adrian Prisacariu. NeRF—: Neural radiance fields without known camera parameters. *arXiv preprint arXiv:2102.07064*, 2021. 2
- [51] Lin Yen-Chen, Pete Florence, Jonathan T. Barron, Alberto Rodriguez, Phillip Isola, and Tsung-Yi Lin. iNeRF: Inverting neural radiance fields for pose estimation. In *IROS*, 2021. 2
- [52] Yoonwoo Jeong, Seokjun Ahn, Christopher Choy, Animesh Anandkumar, Minsu Cho, and Jaesik Park. Self-calibrating neural radiance fields. In *ICCV*, 2021. 2
- [53] Chen-Hsuan Lin, Wei-Chiu Ma, Antonio Torralba, and Simon Lucey. Barf: Bundle-adjusting neural radiance fields. In *ICCV*, 2021. 2

- [54] Mark Boss, Raphael Braun, Varun Jampani, Jonathan T. Barron, Ce Liu, and Hendrik P.A. Lensch. Nerd: Neural reflectance decomposition from image collections. In *ICCV*, 2021. 2
- [55] Pratul P. Srinivasan, Boyang Deng, Xiuming Zhang, Matthew Tancik, Ben Mildenhall, and Jonathan T. Barron. Nerv: Neural reflectance and visibility fields for relighting and view synthesis. In *CVPR*, 2021. 2
- [56] Sai Bi, Zexiang Xu, Pratul Srinivasan, Ben Mildenhall, Kalyan Sunkavalli, Miloš Hašan, Yannick Hold-Geoffroy, David Kriegman, and Ravi Ramamoorthi. Neural reflectance fields for appearance acquisition. *arXiv preprint arXiv:2008.03824*, 2020. 2
- [57] Zhang Chen, Anpei Chen, Guli Zhang, Chengyuan Wang, Yu Ji, Kiriakos N Kutulakos, and Jingyi Yu. A neural rendering framework for free-viewpoint relighting. In *CVPR*, 2020. 2
- [58] Kai Zhang, Gernot Riegler, Noah Snavely, and Vladlen Koltun. Nerf++: Analyzing and improving neural radiance fields. *arXiv preprint arXiv:2010.07492*, 2020. 2
- [59] Konstantinos Rematas, Andrew Liu, Pratul P Srinivasan, Jonathan T Barron, Andrea Tagliasacchi, Thomas Funkhouser, and Vittorio Ferrari. Urban radiance fields. In *CVPR*, 2022. 2
- [60] Julian Ost, Fahim Mannan, Nils Thuerey, Julian Knodt, and Felix Heide. Neural scene graphs for dynamic scenes. In *CVPR*, 2021. 2
- [61] Christopher Xie, Keunhong Park, Ricardo Martin-Brualla, and Matthew Brown. Fig-nerf: Figure-ground neural radiance fields for 3d object category modelling. In *3DV*, 2021. 2
- [62] Sagie Benaim, Frederik Warburg, Peter Ebert Christensen, and Serge Belongie. Volumetric disentanglement for 3d scene manipulation. *arXiv preprint arXiv:2206.02776*, 2022. 2
- [63] Sosuke Kobayashi, Eiichi Matsumoto, and Vincent Sitzmann. Decomposing nerf for editing via feature field distillation. *arXiv preprint arXiv:2205.15585*, 2022. 2
- [64] Bangbang Yang, Yinda Zhang, Yinghao Xu, Yijin Li, Han Zhou, Hujun Bao, Guofeng Zhang, and Zhaopeng Cui. Learning object-compositional neural radiance field for editable scene rendering. In *ICCV*, 2021. 2
- [65] Bing Wang, Lu Chen, and Bo Yang. Dm-nerf: 3d scene geometry decomposition and manipulation from 2d images. *arXiv preprint arXiv:2208.07227*, 2022. 2
- [66] Karl Stelzner, Kristian Kersting, and Adam R Kosiorek. Decomposing 3d scenes into objects via unsupervised volume segmentation. *arXiv preprint arXiv:2104.01148*, 2021. 2
- [67] Hongyi Xu, Thiemo Alldieck, and Cristian Sminchisescu. Unsupervised discovery of object radiance fields. In *ICLR*, 2022. 2
- [68] Cameron Smith, Hong-Xing Yu, Sergey Zakharov, Fredo Durand, Joshua B Tenenbaum, Jiajun Wu, and Vincent Sitzmann. Unsupervised discovery and composition of object light fields. *arXiv preprint arXiv:2205.03923*, 2022. 2
- [69] Nelson Max. Optical models for direct volume rendering. *IEEE TVCG*, 1995. 3
- [70] Piotr Bojanowski, Armand Joulin, David Lopez-Paz, and Arthur Szlam. Optimizing the latent space of generative networks. *arXiv preprint arXiv:1707.05776*, 2017. 3
- [71] Chris J Maddison, Andriy Mnih, and Yee Whye Teh. The concrete distribution: A continuous relaxation of discrete random variables. *arXiv preprint arXiv:1611.00712*, 2016. 4
- [72] Eric Jang, Shixiang Gu, and Ben Poole. Categorical reparameterization with gumbel-softmax. *arXiv preprint arXiv:1611.01144*, 2016. 4
- [73] Peter Hedman, Pratul P. Srinivasan, Ben Mildenhall, Jonathan T. Barron, and Paul Debevec. Baking neural radiance fields for real-time view synthesis. In *CVPR*, 2021. 5
- [74] Liang-Chieh Chen, Yukun Zhu, George Papandreou, Florian Schroff, and Hartwig Adam. Encoder-decoder with atrous separable convolution for semantic image segmentation. In *ECCV*, 2018. 5
- [75] Marius Cordts, Mohamed Omran, Sebastian Ramos, Timo Rehfeld, Markus Enzweiler, Rodrigo Benenson, Uwe Franke, Stefan Roth, and Bernt Schiele. The cityscapes dataset for semantic urban scene understanding. In *CVPR*, 2016. 5
- [76] Mathilde Caron, Hugo Touvron, Ishan Misra, Hervé Jégou, Julien Mairal, Piotr Bojanowski, and Armand Joulin. Emerging properties in self-supervised vision transformers. In *ICCV*, 2021. 5
- [77] Zhou Wang, Alan C Bovik, Hamid R Sheikh, and Eero P Simoncelli. Image quality assessment: from error visibility to structural similarity. *IEEE TIP*, 2004. 5
- [78] Richard Zhang, Phillip Isola, Alexei A Efros, Eli Shechtman, and Oliver Wang. The unreasonable effectiveness of deep features as a perceptual metric. In *CVPR*, 2018. 5
- [79] Johannes L Schonberger and Jan-Michael Frahm. Structure-from-motion revisited. In *CVPR*, 2016. 8